A slowly activating voltage-dependent K^+ current in rat pituitary nerve terminals

Gordan Kilic, Andreas Stolpe and Manfred Lindau*

Department of Molecular Cell Research, Max-Planck-Institute for Medical Research, Jahnstrasse 29, 69120 Heidelberg, Germany

1. A novel slowly activating voltage-dependent K^+ current was observed in isolated nerve terminals from rat neurohypophysis using the whole-cell configuration of the patch-clamp technique.

2. The activation kinetics of the slow current could be fitted assuming Hodgkin–Huxley-type kinetics, an exponential, n, of 1·3 and activation time constants decreasing from 4 s at −50 mV to 0·7 s at +40 mV.

3. A positive shift of reversal potential was observed when $[K^+]$ was increased in the bath solution. The current is carried mainly but not exclusively by K^+ ions.

4. When intracellular free $[Mg^{2+}]$ was low (~60 μM), average current density was 74 pA pF^{-1} at membrane potentials around 0 mV. In 83% of nerve terminals current amplitude was >20 pA pF^{-1}.

5. The slow current was never observed when the pipette contained 4·6 mM free Mg^{2+}. At a physiological level of free Mg^{2+} (0·5 mM) the average current density was 16 pA pF^{-1}.

6. When nerve terminals were analysed after patch-clamp experiments for vasopressin content by immunodetection, no difference in current amplitude was found between the terminals containing vasopressin and all analysed terminals.

7. The voltage dependence of activation was fitted by a Boltzmann equation giving a half-activation potential of −37 mV and a slope factor of about 9 mV.

8. Tail current deactivation kinetics was biexponential with time constants of 0·12 and 1·5 s. Kinetics was dependent on the duration of the activating pulse.

9. Noise analysis of the slow current indicated a single-channel current of 0·33 pA at +6 mV, corresponding to a single-channel conductance of 4·3 pS.

10. This is the first demonstration of a current similar to the slow K^+ current, I_{Ks}, in a neurone, suggesting that a protein similar to the I_{Ks}-inducing channel protein I_{sK} (minK) may be present in peptidergic nerve terminals.

11. The activation properties are consistent with a role of the slow current in inhibition of excitability, at least at the level of the nerve terminal.

Nerve terminals of magnocellular neurones are located in the neurohypophysis, where they secrete oxytocin (OT) or arginine vasopressin (AVP) when electrically stimulated. Upon depolarization, Ca^{2+} entry through voltage-activated calcium channels leads to the exocytotic fusion of secretory granules with the plasma membrane of the nerve terminal (Fidler Lim, Nowycky & Bookman, 1990). The excitability of pituitary nerve terminals is regulated by a variety of voltage-activated channels (Lemos & Nowycky, 1989; Thorn, Wang & Lemos, 1991; Bielefeldt, Rotter & Jackson, 1992; Wang, Thorn & Lemos, 1992). A fast transient K^+ current (A-current, $I_{K(A)}$) may be the major current responsible for terminal repolarization after a spike (Thorn *et al.* 1991).

The electrical activity of magnocellular neurones occurs in bursts (Poulain & Wakerley, 1982) and the bursting activity is required for optimal peptide release (Cazalis, Dayanithi & Nordmann, 1985). These bursts are sustained by plateau potentials lasting several seconds (Andrew & Dudek, 1983). In vasopressin neurones phasic activity was observed in which bursts were separated by silent periods with a duration of seconds (Poulain & Wakerley, 1982). At the level of the

* To whom correspondence should be addressed.

Table 1. Composition (mM) of pipette and external solutions

Constituent	Pipette solution			External solution		
	P1	P2	P3	E1	E2	E3
NMG-Cl	—	—	—	100	100	100
Potassium glutamate	145	141	131	—	—	—
KCl	9	9	9	5	5	15
NaCl	4·6	4·6	4·65	40	25	15
$MgCl_2$	1·8	6·4	2·5	1	1	1
ATP-Na_2	4·6	1·8	2·33	—	—	—
EGTA	0·09	0·09	0·09	—	—	—
HEDTA	—	—	—	—	2	2
$CaCl_2$	—	—	—	2	1	1
D-Glucose	—	—	—	15	10	10
Hepes	9	9	9	10	10	10
4-AP	—	—	—	—	20	20
cAMP	0·03	0·03	0·03	—	—	—
$CdCl_2$	—	—	—	—	0·1	0·1
Free [Ca^{2+}]	—	—	—	—	0·02	0·02
Free [Mg^{2+}]	0·06	4·6	0·5	—	0·2	0·2

The pH of all solutions was finally adjusted to 7·25 with NaOH (P1–P3) or HCl (E1–E3). Osmolality of all solutions was adjusted to 300 mosmol kg^{-1}. Free [Mg^{2+}] of P1, P2 and P3 and free [Ca^{2+}] of E2 and E3 were estimated using a computer program as described previously (Tatham & Lindau, 1990). Values of free [Ca^{2+}] were confirmed by measurements using a calcium electrode.

nerve terminal, sustained repetitive stimulation for more than 5 s leads to inactivation of excitability (Bourque, 1990). These phenomena require long-lasting K^+ currents with kinetics of several seconds that are activated at potentials around −40 mV. One current with the desired property is the Ca^{2+}-activated K^+ current ($I_{K(Ca)}$) and it was suggested that this current may be involved in termination of action potential bursts or regulation of interburst interval duration (Wang *et al.* 1992). In the present study, we demonstrate the presence of an additional current in pituitary nerve terminals, which may contribute to the modulation of excitability and peptide release. This current is activated by depolarization and has activation kinetics of the order of seconds.

METHODS

Preparation of nerve terminals

Nerve terminals were prepared from adult Sprague–Dawley rats as described previously (Cazalis, Dayanithi & Nordmann, 1987) with some modifications. After decapitation of the animal using a guillotine, the neurohypophysis was isolated and placed in physiological saline at 37 °C containing (mM): 140 NaCl, 5 KCl, 5 $NaHCO_3$, 1 $MgCl_2$, 0·5–2·2 $CaCl_2$, 10 D-glucose, 0·01% (w/v) bovine serum albumin and 10 Hepes–NaOH (pH 7·25). The neural lobe was isolated under a microscope and briefly homogenized in 100 μl of buffer containing (mM): 270 D-sucrose, 0·01 EGTA and 10 Hepes. The pH was adjusted to 7·25 using *N*-methyl-D-glucamine hydroxide (NMG-OH). The homogenate, containing nerve terminals detached from their axons, was transferred into a recording chamber, the bottom of which was a glass coverslip. The terminals were allowed to settle on the bottom for about 1 min and then the chamber was washed using the bath perfusion system with 10 μl solution E1, which was also used as standard solution for electrophysiological measurements (see Table 1). Under the microscope, nerve terminals appeared as smooth spherical bodies with diameters of 2–15 μm. Terminals with diameter >9 μm were used for patch-clamp experiments within 2–3 h after the rat was killed. To confirm that the large spherical objects were indeed nerve terminals and not cells (such as melanotrophs, which were also present in the homogenate), in some experiments the DNA-staining fluorescent dye DAPI (Molecular Probes, Eugene, OR, USA) was included in the pipette solution. Following patch rupture and diffusion of the dye into the nerve terminal, a weak homogeneous fluorescence was seen under the microscope. In contrast, when cells present in the homogenate were patched as controls, DAPI displayed a bright intense fluorescence localized in a region of about 2 μm in diameter, very probably the nucleus.

Electrophysiology

The whole-cell patch-clamp technique was used to study isolated nerve terminals using the internal (pipette) and external solutions listed in Table 1. Pipette solutions were prepared to contain low (P1), high (P2) or physiological (P3) concentrations of free Mg^{2+}, keeping the concentration of the Mg–ATP complex approximately constant (~2 mM). External solutions E2 and E3 contained 4-aminopyridine (4-AP) to block the A-current and 100 μM Cd^{2+}. Owing to the high affinity of HEDTA for Cd^{2+}, the free concentration of Cd^{2+} was probably very low. A Ca^{2+}–HEDTA mixture, which buffered free [Ca^{2+}] to ~20 μM, was included in solutions E2 and E3. At this concentration Ca^{2+} channel currents, due to Ca^{2+} ions and also to other ions such as Na^+, are minimized (Almers & McCleskey, 1984).

Borosilicate glass (Hilgenberg, Malsfeld, Germany) pipettes were coated and fire polished to obtain a resistance of 4–12 MΩ. Seal formation and whole-terminal configuration were always attained

in solution E1. The bath electrode with a Ag–AgCl pellet was filled with 1 M KCl and immersed in the bath solution via an agar bridge. The liquid junction potential present at the pipette tip when immersed in solution E1 was measured using a bath electrode and bridge connection, both filled with 3 M KCl. All potentials were corrected for the measured liquid junction potential of 14 mV. Nerve terminals were perfused with different solutions by gravity through several barrels. The barrels terminated in a glass tube (diameter, ~1 mm) located at a distance of ~1 mm from the patched nerve terminal. One barrel contained solution E1 and other barrels solutions E2 and E3. The flow of solutions through the barrels was controlled by electric valves connected to a home-built controller. This device allowed the flow of solution from only one barrel at any time.

Whole-terminal currents were measured with an ATARI Mega/STE-controlled (E9Screen 4.10) EPC9 patch-clamp amplifier (HEKA Electronics, Lambrecht/Pfalz, Germany) in voltage-clamp mode. In whole-terminal configuration, compensation of membrane capacitance and access resistance was performed using the automatic compensation of the EPC9. Capacitance and access resistance were in the range 1·8–8 pF and 7–15 MΩ, respectively. Voltage pulses were produced and analog current outputs sampled by a second ATARI Mega/STE equipped with 12 bit D/A and A/D converters (Issendorff, Sarstedt, Germany) programmed in Omicron BASIC using home-written assembly language routines operating the A/D–D/A board. Current output was filtered with a low-pass eight-pole Bessel filter (LPF 902; Frequency Devices, Haverhill, MA, USA) at cut-off frequencies of 500 or 1250 Hz and sampled every 1 or 0·4 ms, respectively.

In all experiments, a holding potential of −84 mV was applied. Due to the required long pulse durations (up to 20 s) and the limited lifetime of currents, a standard $P/4$ method was not suitable for leak subtraction. We therefore used the following method. A 20–50 ms negative pulse with one-quarter of the amplitude of the test pulse was given 1–3 s before the actual command pulse. Recordings were stored on floppy disk and transferred to a Macintosh computer, where leak subtraction and data analysis were performed using the program IGOR (WaveMetrics, Lake Oswego, OR, USA).

For leak subtraction, the current during the short negative pulse was averaged for times later than 3 ms after the onset of the pulse to avoid contribution from incompletely compensated capacitive currents. The leak current obtained by this method was scaled by a factor of four to estimate the leak current during the test pulse, which was then assumed to be time independent. In double-pulse experiments, the leak current was scaled with an appropriate factor depending on the particular potentials used.

Double-pulse protocols were used to measure the tail currents. To obtain current–voltage relationships the amplitude of the activating pulse was +90 mV (activation potential, +6 mV). The second step was given to variable test potentials between −104 and −34 mV. The tail current amplitude was measured 2–3 ms after the voltage step, again to avoid a contribution from uncompensated capacitive currents. To correct for variability among individual nerve terminals and for run-down during an experiment, the tail current amplitude was divided by the final slow current developing during the activation pulse. The final amplitude of the slow current was taken as the difference between the total final current and the initial rapidly activated current. These relative tail current values (I_t) were plotted as a function of test potential and fitted with a straight line. The reversal potential was determined as the intersection of this line with the abscissa.

To obtain an activation curve, the activation potential was varied from −74 to +36 mV, after which the voltage was stepped to a fixed test potential of −34 mV. The current amplitude at the beginning of the second pulse was measured as described above. Here, to correct for a run-down effect, the steady-state current at −34 mV was used for normalization. Since the steady state was not reached during the 5 s test pulse when the activation pulse was more negative, the steady-state currents at −34 mV following a prepulse to potentials higher than −34 mV were plotted as a function of time and fitted by a straight line. The tail current amplitudes were then normalized using the time dependence of run-down given by the fit. Data were presented as mean values ± standard deviation, unless otherwise indicated. Experiments were performed at room temperature (22–24 °C).

Immunodetection of vasopressin

Individual nerve terminals were analysed for vasopressin content using a technique similar to that developed by Wang, Treistman & Lemos (1993). Nerve terminals were sucked into the pipette after patch-clamp recording was finished and the pipette containing the disrupted nerve terminal was stored at −20 °C until use. Individual pipettes were thawed and the tip, which contained an air bubble after thawing, was broken off by touching it gently with a sheet of paper. The shaft of the pipette was also broken off close to the point where solution was present. The contents were aspirated into a C10 tip (Gilson) using a 20 μl pipette. The aspirated solution was then slowly applied to the nitrocellulose membrane while suction was applied from a vacuum pump. To perform this technique in a suitable manner, circles with an inner diameter of 1–1·5 mm (corresponding to an area of ~3 mm^2) were manually marked on a nitrocellulose membrane filter (Hybond-C-extra; Amersham) using silicone rubber (RTV 615A/B; GE Silicones) and the silicone was cured for 1 h at 70 °C.

After sample application the membrane was dried at room temperature and transferred for blocking into TBS (Tris-buffered saline: 135 mM NaCl, 10 mM Tris–HCl, pH 7·4) containing 5% blocking agent (Amersham; NIP551 of the ECL kit). Blocking was performed for 1 h, followed by two washes, first with TBS and second with PBST (phosphate-buffered saline with Tween: 0·1 M NaH_2PO_4, 0·1 M Na_2HPO_4, 0·1% Tween 20 (Sigma), pH 7·4). The incubation with primary anti-vasopressin antibody from rabbit (Quartett, Berlin, Germany) was performed for about 1 h (dilution 1 : 2000 in PBST). After three washes the membrane was incubated for 1 h with the secondary biotinylated goat anti-rabbit immunoglobulin G antibody (Sigma) (dilution, 1 : 20 000 in PBST) followed by three washes and another 1 h incubation with avidin–horseradish peroxidase (Sigma) (dilution, 1 : 20 000 in PBST). Detection of peroxidase activity was performed using the ECL system (Amersham) according to the instructions of the manufacturer.

On each membrane, control amounts of Arg^8-vasopressin (Bachem, Heidelberg, Germany) or oxytocin (Bachem) were applied in different amounts between 0·25 and 10 pg. The X-ray films (X-OMAT AR; Kodak) were digitized using a CCD camera and analysed using NIH Image (National Institutes of Health, USA). For analysis, square regions of interest were defined and the signal intensity was measured as the sum of the intensities of all pixels within the region of interest minus the background, determined as the sum of intensities in a region of interest of the same size in a field containing no signal. The known vasopressin concentrations were used to generate calibration curves relating signal intensities to vasopressin concentrations.

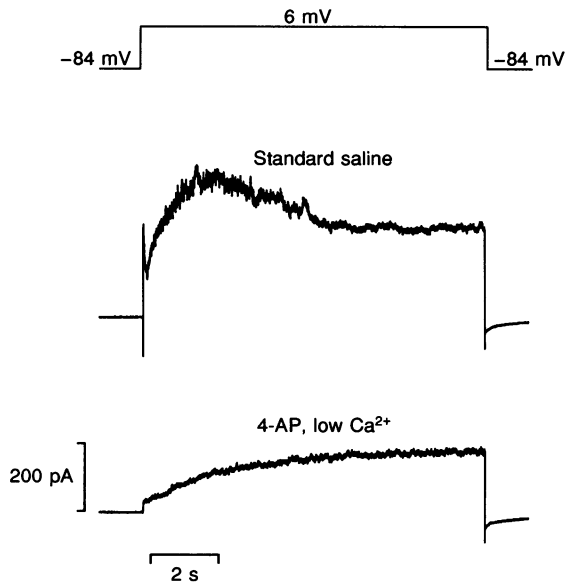

Figure 1. Isolation of slow outward current in pituitary nerve terminals

The nerve terminal was held at −84 mV in the whole-cell configuration. In both traces, a depolarizing pulse was given to +6 mV for 10 s, as indicated in the voltage protocol (top). Pipette solution P1, which contained ~60 μM free Mg^{2+}, was used for both traces. In the upper trace, the external solution was E1 (standard saline solution). In the lower trace, the external solution was changed to E2, which contained 4-AP and had a low free [Ca^{2+}]. In this solution, the main current component is a slowly activating outward current. The membrane capacitance of the terminal was 2·4 pF. Sampling time was 0·4 ms.

RESULTS

A slowly activating voltage-dependent outward current

Figure 1 (upper trace) shows the current measured after a prolonged depolarization in a pituitary nerve terminal in the whole-terminal configuration using standard solutions in the pipette (P1) and bath (E1). The initial fast increase reflects activation of $I_{K(A)}$, which inactivates within 300 ms. The subsequent increase in outward current shows large fluctuations, indicating that it may reflect activation of large Ca^{2+}-activated K^+ channels activated by an influx of Ca^{2+} through voltage-activated Ca^{2+} channels (Wang *et al.* 1992). The outward current is partly inactivated within a couple of seconds. A steady state of the total current is reached after about 5 s and a slow tail current is observed upon repolarization to the holding potential. The recording also shows a marked reduction in current fluctuations associated with the decrease (2–4 s after onset of depolarization), suggesting that the total current is the sum of at least two different channel types. To isolate the current with small fluctuations, a bath solution containing 20 mM 4-AP to block $I_{K(A)}$ and 20 μM free Ca^{2+} to minimize Ca^{2+} entry was perfused into the dish (Fig. 1, lower trace). The remaining component is an outward current with very slow activation kinetics and a characteristic slow tail current upon repolarization to the holding potential. This current is hereafter referred to as the 'slow current'.

To quantify the size of the slow current, its amplitude was measured at the end of a 5 s depolarizing pulse of +90 mV amplitude given from the holding potential of −84 mV in

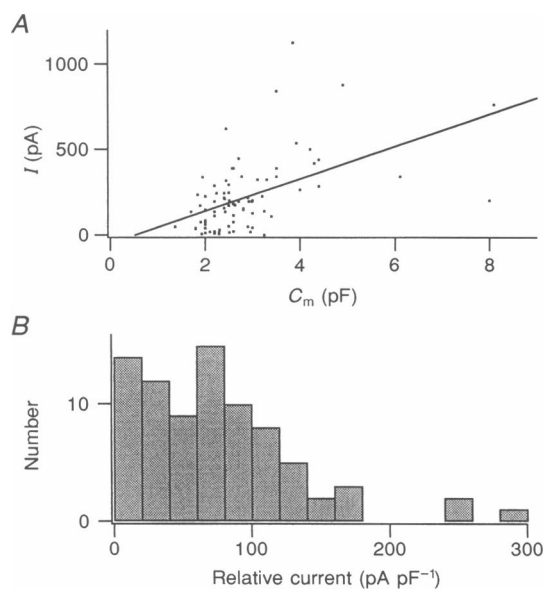

Figure 2. Amplitude of the slow current in pituitary nerve terminals determined using solutions P1 and E2

A, current amplitudes (dots) of 81 nerve terminals were plotted *versus* terminal capacitance (C_m). The straight line represents a linear fit with a slope of 94 pA pF^{-1} (correlation coefficient, 0·52). *B*, frequency distribution of current amplitudes normalized to total membrane capacitance using a bin width of 20 pA pF^{-1}. Mean value was 73·6 ± 58·3 pA pF^{-1} (± S.D., $n = 81$).

the presence of solution E2. Figure 2*A* shows the current amplitude as a function of nerve terminal capacitance. In spite of large scatter, linear regression indicates that the current is proportional to the membrane area of the nerve terminals with a slope of about 94 pA pF^{-1}. Given a specific capacitance of pituitary nerve terminals of 7·6 fF μm^{-2} (Rosenboom & Lindau, 1994), this corresponds to a current density of ~0·7 pA μm^{-2} for the slow current. Figure 2*B* shows the frequency distribution of current densities normalized to the terminal capacitance. In 83% of the terminals current density was >20 pA pF^{-1}. The mean (±S.E.M.) current density was 73·6 ± 6·4 pA pF^{-1} ($n = 81$), corresponding to ~0·6 pA μm^{-2}.

Analysis of vasopressin content

It is believed that vasopressin and oxytocin are produced in separate cells (Swaab, Nijveldt & Pool, 1975; Vandesande & Dierickx, 1975), suggesting that there should be two types of pituitary nerve terminals, one containing vasopressin and the other oxytocin. To determine whether the presence or absence of the slow current was correlated with a nerve terminal being of the vasopressin or oxytocin type, individual nerve terminals were aspirated into the patch pipette after the electrophysiological experiment and analysed for vasopressin content using an immunodetection technique similar to that described previously (Wang *et al.* 1993). Figure 3*A* shows such an experiment. Lane 1 shows signals from different amounts of vasopressin as indicated. No significant signal is observed when the same amounts of oxytocin are used (lane 2). Lane 3 shows signals from different test samples. To quantify the detected amounts of vasopressin, the film was digitized and the intensities in the different spots were measured. Figure 3*B* shows the relationship between the measured signal and the vasopressin content obtained from lane 1. This curve was then used to convert the intensities of lane 3 into vasopressin amounts, which are indicated to the right of lane 3. A nerve terminal was counted as vasopressin positive if more than 1 pg vasopressin was estimated, since this level was significantly different from background in all experiments. The frequency distribution of current densities in these vasopressin-positive nerve terminals is shown in Fig. 3*C*. This distribution is obviously very similar to the total distribution (Fig. 2*B*), suggesting that there is no correlation between the size of the slow current and the vasopressin content of a nerve terminal.

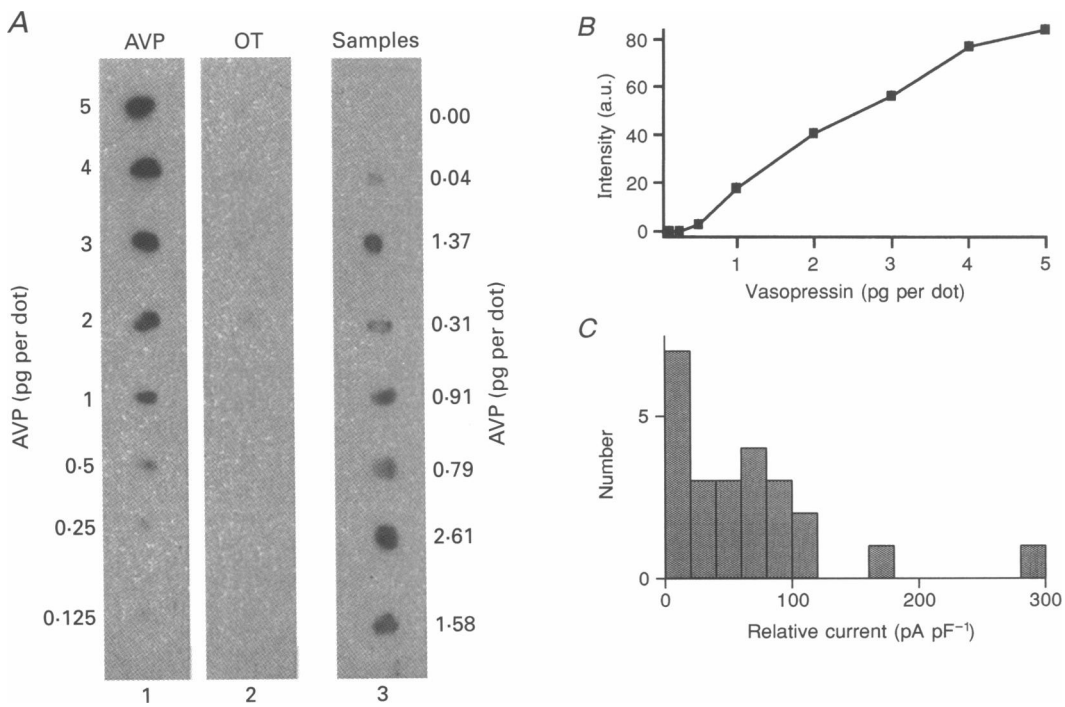

Figure 3. Analysis of nerve terminals for vasopressin content

A, digitized film indicating variable amounts of vasopressin. Lane 1, calibration with defined vasopressin (AVP) amounts as indicated on the left; lane 2, no signals were obtained when the same amounts of oxytocin (OT) were applied; lane 3, the different samples from individual pipettes generated variable intensities, which were converted into AVP amounts using the calibration curve shown in *B*. *B*, AVP calibration curve plotting dot intensities (arbitrary units, a.u.) *versus* AVP amounts from data of lane 1 in *A*. The graph shows that amounts >1 pg are clearly detectable. Nerve terminals were counted as vasopressin positive when at least 1 pg was detected. *C*, frequency distribution of current densities in the vasopressin-positive nerve terminals.

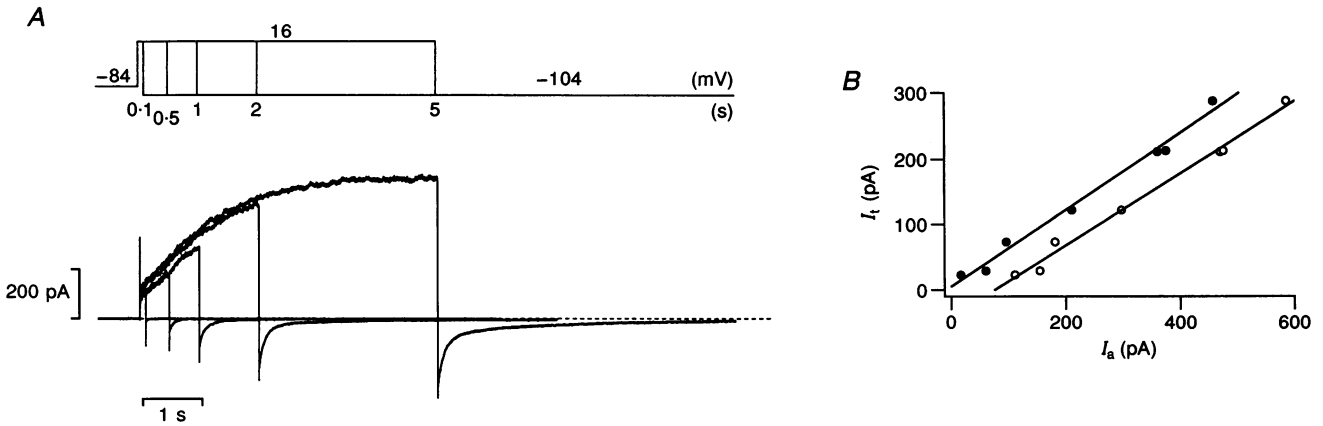

Figure 4. Relationship between activation of slow current and tail current amplitude

A, voltage pulses of different durations were given to a nerve terminal in the whole-cell configuration. The durations of pulses are indicated in seconds. Holding potential was −84 mV. Activation and deactivation potentials were 16 and −104 mV, respectively. Sampling time was 0·4 ms. During the shortest pulse of 0·1 s, the initial fast increase is followed by a very small slow increase and a correspondingly small slow tail current. *B*, amplitudes of slow tail currents (I_t) were determined by extrapolation of single- or double-exponential fits to the slow tail current starting 3 ms after repolarization. I_t values are plotted *versus* current amplitudes at the end of the activation pulse (I_a) (○) and fitted with a straight line. Tail amplitudes are also plotted *versus* the differences between final and initial current during the activating pulse as a measure of the slow component (●). The linear fit to these data points passes close to the origin, indicating that the fast initial increase in outward current does not activate the slow tail current.

Activation and tail currents

As shown in Fig. 1, an inward tail current occurs upon repolarization to −84 mV. To characterize the relationship of this tail current to activation of the slow current, a different pulse protocol was used (Fig. 4*A*, upper panel). Activating pulses of variable duration were given to a potential of +16 mV (100 mV amplitude) and the potential was then stepped to −104 mV, where tail currents were larger.

At high activation potentials (above 0 mV), as used here, the slow rise of the slow current was almost always (47 out of 50 terminals) preceded by a significant initial rapid increase in outward current (Fig. 4*A*, lower panel). After the 0·1 s

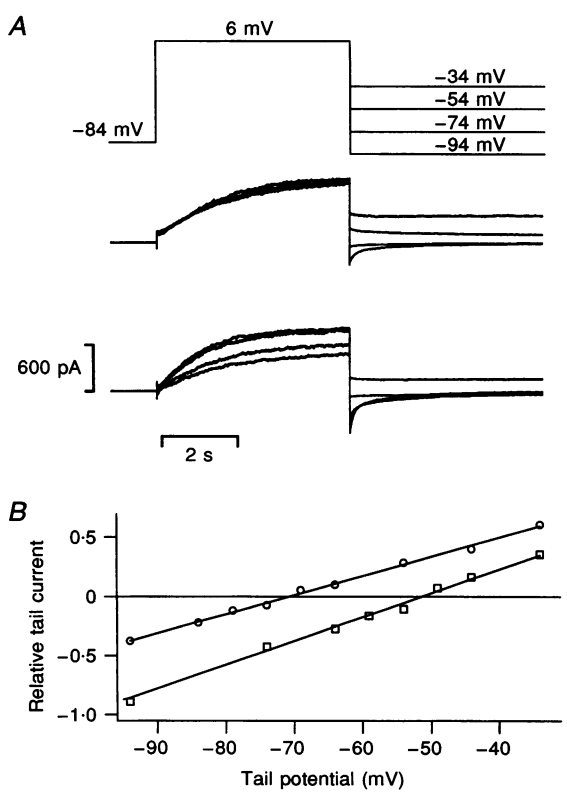

Figure 5. Voltage dependence of tail current amplitudes

A, top panel shows double-pulse protocol; potentials are indicated in millivolts. Upper current traces, bath solution E2, which contained 5 mM K^+; lower current traces, bath solution E3, which contained 15 mM K^+. The two experiments were done using different nerve terminals. Note that the variable size of currents during the first pulse in the lower traces reflects run-down. *B*, to correct for run-down, tail current amplitudes were normalized to the final amplitudes of the first pulse and plotted *versus* the potential of the second pulse. Data points were fitted with straight lines, giving reversal potentials of −70·8 mV in solution E2 (○) and −51·4 mV in solution E3 (□). Terminal capacitances were 3·5 and 5·6 pF, respectively.

depolarization the tail current at repolarization contained mainly a fast component with a time constant < 2 ms. We did not determine whether this component was due to the rapidly activating current or to a maladjustment of the capacitance compensation. As the duration of depolarization increased, a slow tail current became apparent. Its amplitude increased in parallel with the slow current activation. Figure 4*B* shows the relationship between the amplitude of the slow tail current (I_t) and the current at the end of the activating pulse (I_a) (Fig. 4*B*, ○). The relationship is approximately linear but shifted on the abscissa by about 60 pA from the origin. When the rapidly activating current is subtracted from I_a (Fig. 4*B*, ●) the data points are well fitted by a straight line which passes close to the origin, indicating that the tail current increases in proportion to activation of the slow current. The fast component thus appears to be approximately constant throughout the pulse and does not give rise to the slow tail current.

Voltage dependence of tail currents

To characterize the voltage dependence of the open channels, tail currents were measured at different potentials after 5 s activating pulses to +6 mV (Fig. 5*A*). To correct for run-down during the experiment, the tail current amplitudes were normalized to the size of the activating current. These measurements were done using solutions E2, which contained 5 mM K^+ (upper family of traces), and E3, which contained 15 mM K^+ (lower family of traces). The data points could, in both cases, be fitted by a straight line (Fig. 5*B*) giving reversal potentials of −72·5 ± 1·0 mV (mean ± S.E.M., $n = 10$) with solution E2 and −52·3 ± 1·2 mV (mean ± S.E.M., $n = 4$) with solution E3. The positive shift by 18–22·4 mV differs from the 27·8 mV shift expected for perfect K^+ selectivity, indicating that the channels underlying the slow current are preferentially, but not completely, selective for K^+ ions.

The kinetics of tail current deactivation shown in Fig. 6*A* for a potential of −94 mV is not a single exponential, but can be well fitted with a double-exponential decay. The deactivation time constants in this case are 140 ms and 1·4 s. As shown in Fig. 6*B*, the deactivation time constants are not strongly voltage dependent, with mean values of τ_f = 120 ± 50 ms ($n = 34$) for the fast component and τ_s = 1·53 ± 0·78 s ($n = 41$) for the slow component. Both components have similar amplitudes. The relative contribution of the slow decay component increases from ~0·4 around −100 mV to ~0·6 above −70 mV (Fig. 6*C*).

The deactivation after variable activation times was also analysed using the data of Fig. 4. When the duration of activation increased, the deactivation kinetics became slower. For depolarization times up to 0·5 s the deactivation

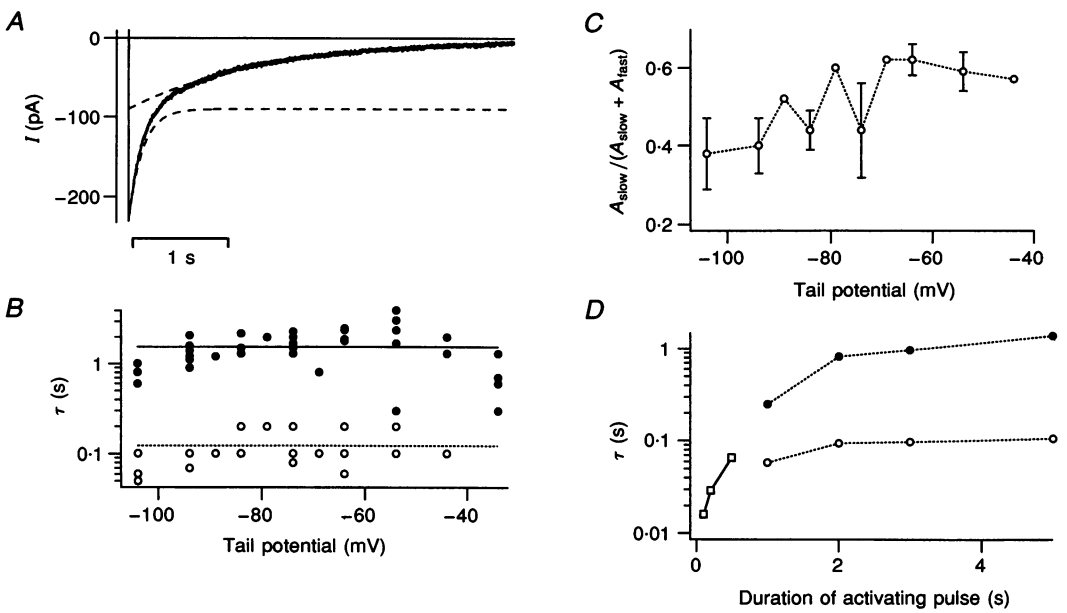

Figure 6. Tail current deactivation

A, tail current recorded at −94 mV following 5 s activation at +6 mV. The decay was well fitted with two exponentials (τ_s = 1·42 s and τ_f = 0·14 s). The fit is indistinguishable from the recorded current. The individual single-exponential decay functions are indicated by dashed lines. *B*, slow (●) and fast (○) deactivation time constants show no strong dependence on repolarization potential. Activation potential was always +6 mV for 5 s. Mean values were 1·53 s for τ_s (continuous line) and 120 ms for τ_f (dashed line). *C*, relative contribution of the slow component plotted *versus* tail potential between −106 and −46 mV, showing an increase from ~0·4 to ~0·6. A_{fast} and A_{slow} denote the amplitudes of the fast and slow components as obtained from the double exponential fit. *D*, deactivation time constants obtained from data of Fig. 4 plotted *versus* duration of activation at +6 mV. □, single-exponential fits; ○, fast component; and ●, slow component of double-exponential fits.

could be fitted by a single exponential. At longer depolarizations a double-exponential fit was necessary and sufficient (see above). The dependence of deactivation kinetics on the duration of the activating pulse (Fig. 6*D*) suggests that conformational changes occur in the channels after opening, leading to additional states which are not associated with a conductance change but are reflected in the changed deactivation kinetics with increasing activation time.

Voltage dependence of activation

To characterize the voltage dependence of activation, tail current amplitudes were measured at −34 mV after 3 ms, preceded by 5 s activation pulses to different potentials. The value of −34 mV was chosen because it is positive enough for substantial activation of the slow current to occur, making it possible to correct for run-down using the steady-state currents. It is negative enough for the current not to be strongly contaminated by the rapidly activating current mentioned above. Figure 7*A* shows a family of traces measured with increasing activation potentials. It should be noted that for low activation potentials the steady state of the current is not fully attained at the end of the second pulse. In these cases, the final current can thus not be used as a measure of active channels in the nerve terminal. However, upon a voltage step from a potential more positive than −34 mV, a steady state was attained rapidly. To correct for run-down, only the steady-state of the second pulse following activation pulses more positive than −34 mV was plotted as a function of time in the whole-cell configuration (Fig. 7*B*) and a straight line was fitted to the data points. For the other pulses, the interpolated steady-state current given by this line for the time of the pulse was used for normalization.

The normalized tail current amplitudes are plotted as a function of activation potential in Fig. 7*C* (○). The data points could be fitted using a Boltzmann-type equation (Fig. 7*C*, continuous line). In this experiment a half-activation potential, $V_{½}$, of −42 mV, and a slope factor, S, of 7·7 mV, were obtained from the fit. Similar results were obtained in five other nerve terminals, giving mean values of −36·7 ± 5·9 mV for $V_{½}$ and 8·6 ± 1·6 mV for S ($n = 6$). It should be noted, however, that at low activation potentials, a steady state is not fully attained by the end of the 5 s activation pulse. The true half-activation potential is probably slightly more negative and the Boltzmann curve more shallow (larger S). Owing to the limited lifetime of the patch, however, it was not possible to use significantly longer activation pulses.

The activation kinetics of the slow current is characterized by a sigmoidal time course and could be well fitted assuming Hodgkin–Huxley-type kinetics (Fig. 8*A*). The fit is indistinguishable from the recorded current. The voltage dependencies of the time constant, τ, and exponent, n, are shown in Fig. 8*B* and *C*, respectively. τ decreases with

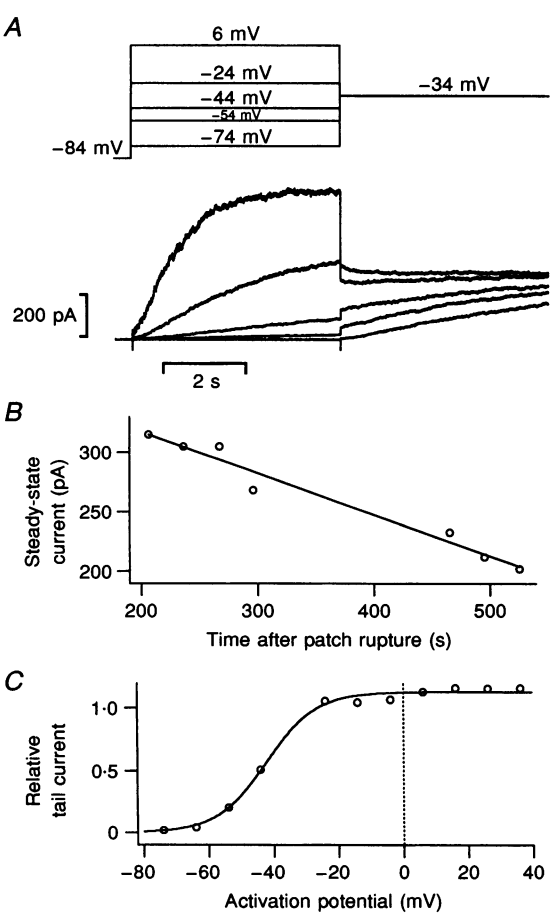

Figure 7. Activation of the slow current

A, the activation curve was measured using the voltage protocol shown in the upper panel. Holding potential was −84 mV. The current traces shown in the lower panel were measured using activation potentials of −74, −54, −44, −24 and +6 mV. Terminal capacitance was 2·5 pF and sampling time was 0·4 ms. Note that for activation potentials lower than −40 mV, the steady state is not fully attained at the end of the second 5 s pulse to −34 mV. *B*, steady-state currents measured at the end of the second pulse following activation potentials ≥ −24 mV (○) are plotted *versus* the time after obtaining the whole-cell configuration. Data points were fitted with a straight line. The fit was used to normalize tail current amplitudes for steady-state current at −34 mV, thus correcting for run-down. *C*, activation curve for tail current amplitudes normalized to steady-state current at −34 mV (○) were fitted using the Boltzmann equation $A = A_0/\{1 + \exp((V_{½} - V)/S)\}$ (continuous line), giving $V_{½} = -42{\cdot}3$ mV and $S = 7{\cdot}7$ mV. A is the tail current amplitude normalized to steady-state current at −34 mV; A_0 is the maximal normalized tail current amplitude as obtained from the fit.

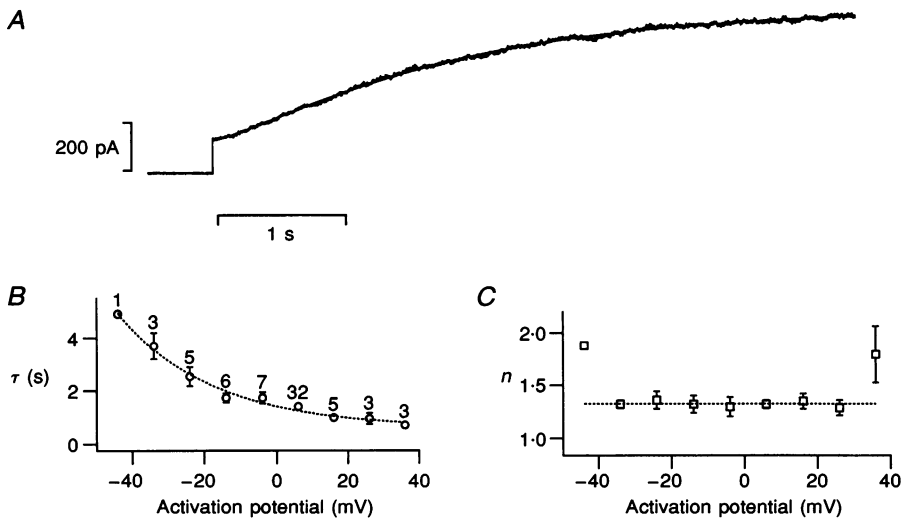

Figure 8. Activation kinetics of the slow current

A, the current activated by a 5 s depolarizing pulse to +6 mV from a holding potential of −84 mV was fitted with a Hodgkin–Huxley-type equation, $I = I_0 + I_1(1 - \exp(-t/\tau))^n$, giving $\tau = 1{\cdot}6$ s and $n = 1{\cdot}3$. I_0 and I_1 are fit parameters: I_0 is the instantaneous current and I_1 is the amplitude of the slow current. τ is voltage dependent (*B*), but n is practically constant (*C*). Data points are presented as means ± S.E.M. Numbers indicate number of measurements. Dotted line in *B* is an exponential fit through the mean values, whereas in *C* it is the mean value obtained by averaging all the individual values.

increasing depolarization, whereas the value of n is more or less constant (mean value, 1·32), indicating that the Hodgkin–Huxley model provides a suitable description for the activation kinetics of the slow current.

Sensitivity to intracellular [Mg^{2+}]

A slowly activating potassium current in heart cells is blocked or inhibited by high concentrations of intracellular Mg^{2+} (Duchatelle-Gourdon, Lagrutta & Hartzell, 1991). To test whether the slow current in nerve terminals is also sensitive to high intracellular [Mg^{2+}], experiments were done using pipette solution P2, which contained about 5 mM free Mg^{2+}. Figure 9 shows such recordings using solution P2 in the pipette and external solution E1 (upper current trace) and solution E2 (lower current trace). The steady-state current in the upper trace is very small and, in the presence of solution E2, no slow current is detectable (lower trace). In a total of twelve terminals internally perfused with solution P2 the slow current was never detectable, suggesting that high intracellular [Mg^{2+}] inhibits the slow current.

To investigate whether the slow current can be activated at physiological levels of intracellular free Mg^{2+}, pipette solution P3, which contained ~0·5 mM free Mg^{2+}, was used. As shown in Fig. 10*A*, development of the slow current is clearly detectable. The mean current density at +6 mV was 16·0 ± 1·9 pA pF^{-1} (mean ± S.E.M., $n = 7$), about 22% of that measured with solution P2 (60 μM free Mg^{2+}). In four terminals the signal-to-noise ratio was high enough to fit the activation kinetics with the Hodgkin–Huxley model, giving $\tau = 2{\cdot}6 \pm 0{\cdot}7$ s (mean ± S.E.M., $n = 4$) and $n = 1{\cdot}2 \pm 0{\cdot}1$

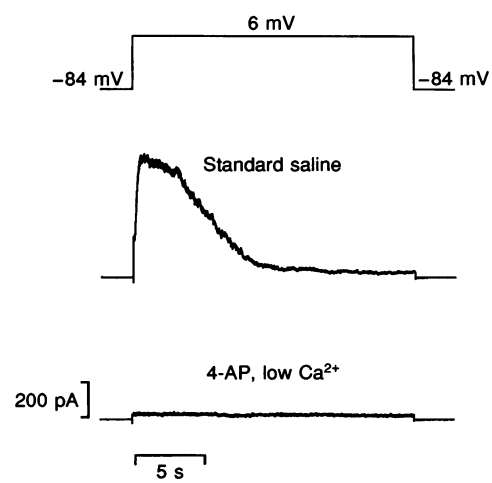

Figure 9. Slow current is not observed when the pipette contains 4·6 mM free Mg^{2+}

The voltage protocol is shown at the top. The pipette solution was P2. Currents from the same terminal were recorded using bath solutions E1 (upper trace) and E2 (lower trace). Note the similarity of the steady-state currents at the end of the pulse in the two different conditions. The sampling time was 1 ms and terminal capacitance was ~2 pF.

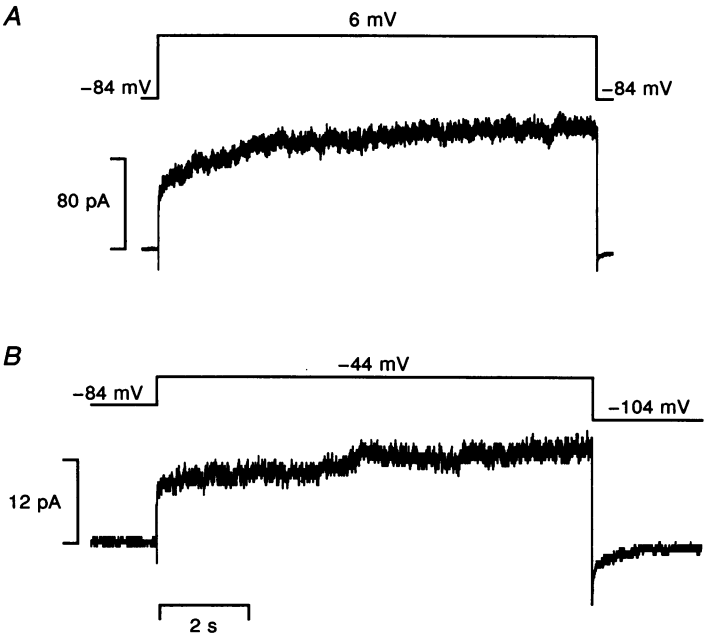

Figure 10. Slow current is observed when the pipette contains 0·5 mM free Mg^{2+}
The pipette solution was P3. *A*, following a fast increase in outward current upon depolarization, activation of the slow current is seen. Terminal capacitance was 3·3 pF. *B*, another terminal (2·2 pF) was depolarized to −44 mV. Note the characteristic slow tail current upon repolarization to −104 mV. Sampling time was 0·4 ms.

(mean ± S.E.M., $n = 4$). These values are close to those measured with solution P2 (Fig. 8*B*). Activation of slow current was also detectable at potentials between −40 and −50 mV and the characteristic slow tail current was observed in response to hyperpolarization to −104 mV (Fig. 10*B*).

Sensitivity to extracellular [K^+]

I_{Kr} is a slowly activating potassium current which is inhibited by complete removal of extracellular K^+ (Scamps & Carmeliet, 1989; Sanguinetti & Jurkiewicz, 1992). The so-called HERG current, which is similar to I_{Kr}, displays the same sensitivity to K^+ (Sanguinetti, Jiang, Curran & Keating, 1995). To test whether the slow current in nerve terminals has the same property, we perfused the bath with K^+-free saline, in which KCl was replaced with D-glucose, thereby keeping osmolarity constant (this solution was otherwise identical to solution E2). The experiment was performed in duplicate and no significant decrease of the slow current was observed in low-K^+ saline (data not shown). We thus conclude that the slow current in nerve terminals is different from I_{Kr} or HERG.

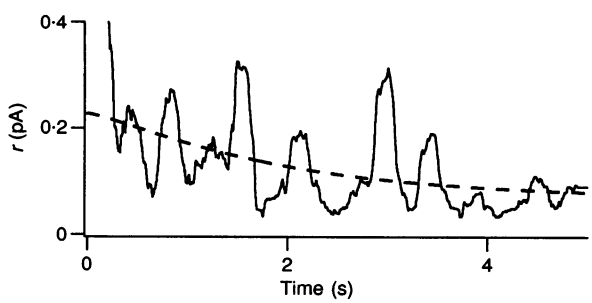

Figure 11. Ratio of variance to the mean of the slow current
The whole-terminal current shown in Fig. 8*A* was used to estimate single-channel current at +6 mV. The fit with the Hodgkin–Huxley model (see Fig. 8*A*) was taken as the mean current. To estimate the variance at any time, the quadratic deviations from the mean were calculated for each data point. The rolling average within a window of 200 ms centred around the time point was then taken as the variance at that time after subtracting the noise measured at the holding potential before the pulse was given. The ratio of variance to the mean current (r) is plotted *versus* time during activation (continuous line). Data at the beginning of the pulse where the slow current was < 35 pA are excluded because the mean current is too small and the ratio becomes unreliable. Current was > 35 pA after 220 ms and the later part was used for noise analysis. The ratio was fitted (dashed line) assuming that the activation kinetics reflects a change in open probability $r = i\{1 - P_{o,max}(1 - \exp(-t/\tau))^n\}$, where τ and n were fixed parameters as determined from kinetics of the slow current (see legend to Fig. 8). Only single-channel current, i, and maximum open probability, $P_{o,max}$, were free fit parameters, giving $i = 0{\cdot}22$ pA and $P_{o,max} = 0{\cdot}7$.

Noise analysis

To characterize the single-channel properties underlying the slow current in nerve terminals, fluctuation analysis was applied. Because of the extremely slow activation kinetics at potentials where the open probability is low, non-stationary noise analysis was performed. An example is shown for the recording illustrated in Fig. 8*A*. The Hodgkin–Huxley fit was taken as the mean current, from which the fast component was subtracted, thus yielding the mean slow current. The ratio of variance to the mean (r) is plotted *versus* time during activation as the continuous line in Fig. 11. The value of r should be equal to the single-channel current (i) only if the open probability is much smaller than 1. Assuming that the activation kinetics reflects the time course of the open probability increase, then r at any time should be $r = i\{1 - P_{o,max}(1 - \exp(-t/\tau))^n\}$, where τ and n are known from the fit to the slow current. The values of i and of the maximal open probability, $P_{o,max}$, were fitted using this equation (dashed line). Data during the first 220 ms at the beginning of the pulse were excluded because the current is very small and the ratio between very small values would have to be calculated. Furthermore, the fit may be slightly different from the true mean current. This analysis was performed on three different recordings at +6 mV, yielding similar results ($i = 0{\cdot}33 \pm 0{\cdot}10$ pA and $P_{o,max} = 0{\cdot}67 \pm 0{\cdot}02$). Given the linear current–voltage relationship (Fig. 5) and the reversal potential of −72·5 mV, this value of i corresponds to a single-channel conductance of $4{\cdot}3 \pm 1{\cdot}2$ pS.

DISCUSSION

In the present study we demonstrate the presence of a slowly activating voltage-dependent outward current in nerve terminals of the rat neurohypophysis.

Ionic selectivity

Reversal potentials of the slow current and Nernst potentials of the main ions in two experimental conditions are given in Table 2. The similarity between the reversal potential, V_{rev}, of the slow current and the Nernst potential, E_K, for K^+ suggests that the current is carried mainly by K^+ ions. However, the potentials do not match exactly, suggesting that K^+ selectivity is not perfect. A positive shift from E_K could be due to a significant permeability of Na^+, NMG^+ or both. Assuming that NMG^+ is impermeant, the reversal potential shift by $20{\cdot}2 \pm 2{\cdot}2$ mV when changing from solution E2 to solution E3 would correspond to a permeability ratio, P_{Na}/P_K, of $0{\cdot}10 \pm 0{\cdot}04$ and the absolute reversal potentials for solutions P2/E2 and P2/E3 should then be $-76{\cdot}8 \pm 3{\cdot}4$ and $56{\cdot}7 \pm 0{\cdot}9$ mV, respectively. These values are not significantly different from the measured values. When we assume instead that NMG^+ is permeant and Na^+ is excluded, then a permeability ratio, P_{NMG}/P_K, of ~0·033 is obtained. Since NMG^+ is unlikely to be more permeant than Na^+, the actual value of P_{NMG}/P_K will be $< 0{\cdot}033$.

Comparison with other K^+ channels in pituitary nerve terminals

In previous studies of pituitary nerve terminals, three types of K^+ currents have been described. A fast, transient outward current, which was classified as $I_{K(A)}$ (Thorn *et al.* 1991; Bielefeldt *et al.* 1992), a current, $I_{K(Ca)}$, carried by large Ca^{2+}-activated K^+ channels (Bielefeldt *et al.* 1992; Wang *et al.* 1992) and a non-inactivating dendrotoxin-sensitive delayed rectifier (D-current) with an activation time constant of ~65 ms at +60 mV (Bielefeldt *et al.* 1992). In one study, the dendrotoxin-sensitive current was observed in about half of the nerve terminals (Bielefeldt *et al.* 1992), whereas other investigators found no evidence for the presence of delayed rectifier (Thorn *et al.* 1991; Wang *et al.* 1992). This discrepancy may be due to presence of D-current in axons of magnocellular neurones that are connected to nerve terminals in the slice preparation (Bielefeldt *et al.* 1992) and not in isolated nerve terminals (Thorn *et al.* 1991; Wang *et al.* 1992) The activation time constant of the slow current described here approaches 700 ms around +40 mV, and is thus much slower than that of the delayed rectifier described by Bielefeldt *et al.* (1992). The single-channel conductance of the D-channel in rat pituitary nerve terminals is 27 pS, whereas we estimate the unit conductance of the slow current using fluctuation analysis to be as small as ~4·3 pS. The slow K^+ current described here is thus different from the previously observed D-current. The slow current requires MgATP, is inhibited by a high free Mg^{2+} concentration in the pipette solution and requires activating pulses with a duration of several seconds. This may explain why the slow current was not discovered in previous studies. The unusually slow activation kinetics allows for the possible involvement of intracellular ion concentration changes or a biochemical process in the activation mechanism. However, in our experiments, the intracellular ion concentrations were set by the composition of the pipette solution and the main permeant ion, K^+, had no effect on current activation. Since the current requires MgATP, a voltage-dependent phosphorylation may be involved, as in the case of calcium facilitation currents and the Ca^{2+}-dependent K^+ current in pituitary nerve terminals

Table 2. Nernst potentials of main ions with pipette solution P1

Ion	Nernst potential (mV) In E2	In E3
K^+	−86·5	−58·8
Na^+	15·2	2·3
NMG^+	+ infinity	+ infinity
Cl^-	−52	−52

The reversal potential of the slow current was $-72{\cdot}5 \pm 1{\cdot}0$ mV in E2 and $-52{\cdot}3 \pm 1{\cdot}2$ mV in E3 (means ± S.E.M.).

(Artalejo, Rossie, Perlman & Fox, 1992; Bielefeldt & Jackson, 1994). However, the activation kinetics could be well fitted using the Hodgkin–Huxley model with a constant value of n over a wide range of potentials, suggesting that the slow activation may simply reflect voltage-dependent conformational changes.

Comparison with other slow K^+ currents

Delayed rectifier potassium currents with extremely slow activation kinetics were originally described in Purkinje fibres (Noble & Tsien, 1969*a*) and were characterized in bull-frog atrial myocytes (Simmons, Creazzo & Hartzell, 1986). In guinea-pig ventricular myocytes (Matsuura, Ehara & Imoto, 1987) the current is composed of two different components, the rapidly activating I_{Kr} and the slowly activating I_{Ks} (Sanguinetti & Jurkiewicz, 1990). The reversal potential of I_{Kr} is indistinguishable from the Nernst potential for K^+. I_{Ks} in atrial cells also reverses close to E_K (Sanguinetti & Jurkiewicz, 1991), but in ventricular cells it reverses at less negative potentials, indicating permeability to other ions also (Sanguinetti & Jurkiewicz, 1990). In contrast to I_{Ks}, I_{Kr} shows some inward rectification, resulting in a voltage-dependent decrease of the peak current above 0 mV (Sanguinetti & Jurkiewicz, 1990). Removal of extracellular K^+ increases I_{Ks} but markedly reduces I_{Kr} (Sanguinetti & Jurkiewicz, 1992). The slow current in nerve terminals shows significant permeability to ions other than K^+, shows no conductance decrease at strong depolarization and is not blocked by removal of extracellular K^+. Thus it does not appear to be related to I_{Kr}, but shows many similarities to I_{Ks}.

The activation kinetics of I_{Ks} in bullfrog atrial myocytes was fitted assuming a Hodgkin–Huxley model with $n = 2$ and a time constant of ~2 s at +5 mV (Simmons *et al.* 1986). In guinea-pig ventricular myocytes, a faster time constant was reported (300 ms at 0 mV), but these experiments were done at higher temperature (35 °C; Matsuura *et al.* 1987). The slow current in pituitary nerve terminals was best described by a Hodgkin–Huxley model with $n = 1{\cdot}32$. In heart cells $n = 2$ provided a better fit than $n = 1$ or $n = 3$, but n was not treated as a free fit parameter. We thus consider the shape of activation for the two currents to be very similar. The activation time constant in nerve terminals is voltage dependent, with values of 1–3 s between +20 and −30 mV, very similar to the activation kinetics of I_{Ks} at room temperature.

Tail currents in guinea-pig ventricular myocytes show a monoexponential decay below −50 mV but a biexponential decay at higher potentials (Matsuura *et al.* 1987). We observed a biexponential decay for the slow current in nerve terminals at all potentials, but the kinetics was affected by the activation protocol.

I_{Ks} shows marked run-down in the presence of 1 mM free Mg^{2+}, whereas at 0·3 mM no run-down was observed (Duchatelle-Gourdon, Hartzell & Lagrutta, 1989). Mg^{2+} blocked the current with an apparent IC_{50} of 0·6 mM and it was suggested that the effect might be mediated by a Mg^{2+}-dependent phosphatase (Duchatelle-Gourdon *et al.* 1991). The slow current in nerve terminals was also absent when the internal solution contained 4·6 mM free Mg^{2+} instead of 60 μM. At 0·5 mM free Mg^{2+}, the current amplitude was reduced by a factor of four to five, indicating that the IC_{50} is somewhat lower than in heart cells. In contrast to heart cells, in nerve terminals, run-down with a time constant of ~10 min was also observed at low free [Mg^{2+}], suggesting that a diffusible cytoplasmic component may be lost during the recording. This discrepancy may be explained by the difference in cell size. The typical capacitance of ventricular myocytes is ~75 pF (Duchatelle-Gourdon *et al.* 1991), ~30 times less than the average 2·8 pF capacitance of the nerve terminals that we used for our recordings. Diffusional exchange between pipette and cell depends on the cell volume (Pusch & Neher, 1988) and should accordingly be ~150 times faster in nerve terminals than in ventricular myocytes. Although, in heart cells, a ~5 times lower pipette resistance may be used, diffusional equilibration leading to run-down will still be about 30 times faster in nerve terminals than in heart cells. The run-down time constant of ~10 min in nerve terminals may thus be prolonged to 5 h in heart cells, suggesting that in heart cells no significant run-down occurs during an experiment because of their large volume.

The half-activation potential in bull-frog atrial cells was about −10 mV, with a slope factor of 12–13 mV (Simmons *et al.* 1986). The current is markedly increased by isoprenaline or forskolin treatment or by internal perfusion with cAMP. This treatment also shifts the half-activation potential to more negative values. The current requires cytosolic ATP and appears to be regulated by kinase/phosphatase-mediated phosphorylation–dephosphorylation mechanisms (Frace & Hartzell, 1993). The half-activation potential of the current in nerve terminals ($V_{½} = -37$ mV) is more negative and the activation curve is steeper ($S \approx 9$ mV) than that of I_{Ks}. Given the sensitivity of the activation curve to phosphorylation or dephosphorylation steps, this discrepancy may reflect differences in charge at particular sites of the channel protein.

The single-channel conductance of I_{Ks} determined in cell-attached recordings is 5·4 pS (Basler, Bennet & Roden, 1990), very similar to the value of 4·3 pS which we estimate from fluctuation analysis for the slow current in nerve terminals. In summary, the slow current studied here shows many similarities to I_{Ks} except for a shift of the activation curve.

A potassium current with slow activation kinetics (I_{sK}) was measured in oocytes following injection of mRNA encoding a single 130 amino acid 15 kDa protein with a single putative hydrophobic transmembrane region (Takumi, Ohkubo & Nakanishi, 1988). The mRNA was originally isolated from kidney and was found in several epithelial

tissues, but was not detected in brain or liver. It was subsequently also localized in heart (Folander, Smith, Antanavage, Bennett, Stein & Swanson, 1990) and it was suggested that the I_{sK} protein (also called minK) is the molecular basis of I_{Ks} (Varnum, Busch, Bond, Maylie & Adelman, 1993). Its activation is sigmoidal and the activation kinetics was described as triexponential, with the slowest component being 38 s. The channel properties varied depending on the species from which the mRNA was obtained (Hice, Folander, Salata, Smith, Sanguinetti & Swanson, 1994). Furthermore, the activation properties depend on intracellular $[Ca^{2+}]$ and temperature (Busch & Lang, 1993). The stoichiometry and subunit composition of the functional channel are not yet unequivocally determined. It was proposed that a functional channel may be composed of at least fourteen subunits (Tzounopoulos, Guy, Durell, Adelman & Maylie, 1995), but other authors concluded that the channel is formed from only two subunits of minK in a complex with one or more other components (Wang & Goldstein, 1995). The current described here is the first slow delayed rectifier with activation times of 1 s or more to be found in neuronal tissue. It appears to be very similar to I_{sK}. The differences in the activation curves may reflect differences in phosphorylation, but may alternatively be due to amino acid substitution involving changes in fixed charge at a particular site. Furthermore, I_{sK} may be combined with other components in a manner different from that in heart cells.

Although the absolute magnitude of the slow current in nerve terminals is small, the current density of ~74 pA pF^{-1} at +6 mV (maximal activation) is higher than in heart cells, where at 0 mV the density is only 15 pA pF^{-1} and the activation level is ~80% (Duchatelle-Gourdon *et al.* 1991). At low free Mg^{2+} concentrations the current density is thus 3–4 times higher in nerve terminals. A current density of 16 pA pF^{-1} was measured in nerve terminals in the presence of physiological free $[Mg^{2+}]$ (0·5 mM). In spite of the high current density in nerve terminals, no minK mRNA was detected in brain tissue (Takumi *et al.* 1988). This suggests that in brain the overall expression level may be small, with high enrichment in specific sites, such as pituitary nerve terminals.

Physiological significance of the slow K^+ current

The slow K^+ current in pituitary nerve terminals is maximally activated at low free Mg^{2+} concentrations. However, significant activation does occur at physiological Mg^{2+} levels, indicating that the current may well be activated *in vivo*. The slow activation kinetics makes it unlikely that the current is involved in repolarization following individual action potentials. Its physiological function should thus be distinct from that of rapidly activating K^+ currents such as delayed rectifier or A-currents.

In heart cells, the role of I_{Ks} is believed to be in repolarization of the long action potentials (Noble & Tsien, 1969*b*; Matsuura *et al.* 1987). In hypothalamic vasopressin neurones, action potentials last only a few milliseconds (Poulain & Wakerley, 1982). However, the action potentials in these cells show a characteristic bursting pattern, with bursts and silent periods on a time scale of several seconds. Long-lasting plateau depolarizations reaching up to −20 mV for 20–90 s were reported in magnocellular neurones (Legendre, Cooke & Vincent, 1982; Theodosis, Legendre & Vincent, 1983). A depolarizing plateau underlies the action potential burst in these cells (Andrew & Dudek, 1983), and it was suggested that the recurrent plateau depolarizations may be the mechanism controlling the phasic bursting activity (Theodosis *et al.* 1983). To terminate the burst, a slow intrinsic hyperpolarizing mechanism is required. It was suggested that the Ca^{2+}-activated K^+ current may contribute to burst termination (Andrew & Dudek, 1983; Wang *et al.* 1992; Bielefeldt & Jackson, 1993).

The slowly activating K^+ current described here has ideal properties to act as an endogenous inhibitory mechanism terminating the burst. During an initial period following depolarization action potentials are initiated normally and the burst is sustained because the current activates only very slowly. After several seconds, however, the plateau depolarization sustaining the burst will be counteracted by activation of the slow current and the burst will be terminated. The half-activation potential is about −40 mV, close to the plateau values.

Although the phasic pattern of activity may be a particular property of vasopressin neurones and is not present in oxytocin neurones (Poulain & Wakerley, 1982), we found no significant differences in current amplitude depending on vasopressin content of the nerve terminals. However, both types of neurones do show burst discharges (Dudek & Andrew, 1985) and thus may have similar mechanisms for burst termination. The difference in bursting patterns between the two types of neurones may reflect different kinetic properties of the mechanisms inducing and modulating excitability. We have not studied a possible dependence of the kinetics of the slow current on vasopressin content.

It is unknown at present whether the slow K^+ current that we observed in the nerve terminals is also present in the cell bodies; it may not have been detected previously because of its unusually slow kinetics. If it is present in the cell bodies, then it may play a role in the termination of action potential bursts. Alternatively, these currents may modulate excitability at the level of the nerve terminal. It has been reported that sustained (>5 s) repetitive stimulation of the neural stalk leads to a gradual increase in latency and eventually failure of spike generation in neurohypophysial nerve terminals (Bourque, 1990). If the pattern of activity reaching the nerve terminal is also associated with a plateau potential underlying the spikes, then the slow K^+ current described here may contribute to the mechanism inactivating excitability at the level of the nerve terminal.

ALMERS, W. & MCCLESKEY, E. W. (1984). Non-selective conductance in calcium channels of frog muscle: calcium selectivity in a single-file pore. *Journal of Physiology* **353**, 585–608.

ANDREW, R. D. & DUDEK, F. E. (1983). Burst discharge in mammalian neuroendocrine cells involves an intrinsic regenerative mechanism. *Science* **221**, 1050–1052.

ARTALEJO, C. R., ROSSIE, S., PERLMAN, R. L. & FOX, A. P. (1992). Voltage-dependent phosphorylation may recruit Ca^{2+} current facilitation in chromaffin cells. *Nature* **358**, 63–66.

BASLER, J. R., BENNET, P. B. & RODEN, D. M. (1990). Time-dependent outward current in guinea pig ventricular myocytes. *Journal of General Physiology* **96**, 835–863.

BIELEFELDT, K. & JACKSON, M. B. (1993). A calcium-activated potassium channel causes frequency-dependent action-potential failures in a mammalian nerve terminal. *Journal of Neurophysiology* **70**, 284–298.

BIELEFELDT, K. & JACKSON, M. B. (1994). Phosphorylation and dephosphorylation modulate a Ca^{2+}-activated K^+ channel in rat peptidergic nerve terminals. *Journal of Physiology* **475**, 241–254.

BIELEFELDT, K., ROTTER, J. L. & JACKSON, M. B. (1992). Three potassium channels in rat posterior pituitary nerve terminals. *Journal of Physiology* **458**, 41–67.

BOURQUE, C. W. (1990). Intraterminal recordings from the rat neurohypophysis *in vitro*. *Journal of Physiology* **421**, 247–262.

BUSCH, A. E. & LANG, F. (1993). Effects of [Ca] and temperature on minK channels expressed in *Xenopus* oocytes. *FEBS Letters* **334**, 221–224.

CAZALIS, M., DAYANITHI, G. & NORDMANN, J. J. (1985). The role of patterned burst and interburst interval on the excitation-coupling mechanism in the isolated rat neural lobe. *Journal of Physiology* **369**, 45–60.

CAZALIS, M., DAYANITHI, G. & NORDMANN, J. J. (1987). Hormone release from isolated nerve endings of the rat neurohypophysis. *Journal of Physiology* **390**, 55–70.

DUCHATELLE-GOURDON, I., HARTZELL, H. C. & LAGRUTTA, A. A. (1989). Modulation of the delayed rectifier potassium current in frog cardiomyocytes by β-adrenergic agonists and magnesium. *Journal of Physiology* **415**, 251–274.

DUCHATELLE-GOURDON, I., LAGRUTTA, A. A. & HARTZELL, H. C. (1991). Effects of Mg^{2+} on basal and β-adrenergic-stimulated delayed rectifier potassium current in frog atrial myocytes. *Journal of Physiology* **435**, 333–347.

DUDEK, F. E. & ANDREW, R. D. (1985). Electrophysiological characteristics of paraventricular and supraoptic neurons. In *Vasopressin*, ed. SCHRIER, R. W., pp. 367–373. Raven Press, New York.

FIDLER LIM, N., NOWYCKY, M. C. & BOOKMAN, J. (1990). Direct measurement of exocytosis and calcium currents in single vertebrate nerve terminals. *Nature* **344**, 449–451.

FOLANDER, K., SMITH, J. S., ANTANAVAGE, J., BENNETT, C., STEIN, R. B. & SWANSON, R. (1990). Cloning and expression of the delayed-rectifier I_{sK} channel from neonatal rat heart and diethylstilbestrol-primed uterus. *Proceedings of the National Academy of Sciences of the USA* **87**, 2975–2979.

FRACE, A. M. & HARTZELL, H. C. (1993). Opposite effects of phosphatase inhibitors on L-type calcium and delayed rectifier currents in frog cardiac myocytes. *Journal of Physiology* **472**, 305–326.

HICE, R. E., FOLANDER, K., SALATA, J. J., SMITH, J. S., SANGUINETTI, M. C. & SWANSON, R. (1994). Species variants of the I_{sK} protein: differences in kinetics, voltage dependence, and La^{3+} block of the currents expressed in *Xenopus* oocytes. *Pflügers Archiv* **426**, 139–145.

LEGENDRE, P., COOKE, I. M. & VINCENT, J. D. (1982). Regenerative responses of long duration recorded intracellularly from dispersed cell cultures of fetal mouse hypothalamus. *Journal of Neurophysiology* **48**, 1121–1141.

LEMOS, J. R. & NOWYCKY, M. C. (1989). Two types of calcium channels coexist in peptide-releasing vertebrate nerve terminals. *Neuron* **2**, 1419–1426.

MATSUURA, H., EHARA, T. & IMOTO, Y. (1987). An analysis of the delayed outward current in single ventricular cells of the guinea-pig. *Pflügers Archiv* **410**, 596–603.

NOBLE, D. & TSIEN, R. W. (1969*a*). Outward membrane currents activated in the plateau range of potentials in cardiac Purkinje fibres. *Journal of Physiology* **200**, 205–231.

NOBLE, D. & TSIEN, R. W. (1969*b*). Reconstruction of the repolarization process in cardiac Purkinje fibres based on voltage clamp measurements of membrane current. *Journal of Physiology* **200**, 233–254.

POULAIN, D. A. & WAKERLEY, J. B. (1982). Electrophysiology of hypothalamic magnocellular neurons secreting oxytocin and vasopressin. *Neuroscience* **7**, 773–808.

PUSCH, M. & NEHER, E. (1988). Rates of diffusional exchange between small cells and a measuring patch pipette. *Pflügers Archiv* **411**, 204–211.

ROSENBOOM, H. & LINDAU, M. (1994). Exo-endocytosis and closing of the fission pore during endocytosis in single pituitary nerve terminals internally perfused with high calcium concentrations. *Proceedings of the National Academy of Sciences of the USA* **91**, 5267–5271.

SANGUINETTI, M. C., JIANG, C., CURRAN, M. E. & KEATING, M. T. (1995). A mechanistic link between an inherited and an acquired cardiac arrhythmia: *HERG* encodes the I_{Kr} potassium channel. *Cell* **81**, 299–307.

SANGUINETTI, M. C. & JURKIEWICZ, N. K. (1990). Two components of cardiac delayed rectifier K^+ current. *Journal of General Physiology* **96**, 195–215.

SANGUINETTI, M. C. & JURKIEWICZ, N. K. (1991). Delayed rectifier outward K^+ current is composed of two currents in guinea pig atrial cells. *American Journal of Physiology* **260**, H393–399.

SANGUINETTI, M. C. & JURKIEWICZ, N. K. (1992). Role of external Ca^{2+} and K^+ in gating of cardiac delayed rectifier K^+ currents. *Pflügers Archiv* **420**, 180–186.

SCAMPS, F. & CARMELIET, E. (1989). Delayed K current and external K in single cardiac Purkinje cells. *American Journal of Physiology* **260**, H393–399.

SIMMONS, M. A., CREAZZO, T. & HARTZELL, H. C. (1986). A time-dependent and voltage-sensitive K^+ current in single cells from frog atrium. *Journal of General Physiology* **88**, 739–755.

SWAAB, D. F., NIJVELDT, F. & POOL, C. W. (1975). Distribution of oxytocin and vasopressin in the rat supraoptic and paraventricular nucleus. *Journal of Endocrinology* **67**, 461–462.

TAKUMI, T., OHKUBO, H. & NAKANISHI, S. (1988). Cloning of a membrane protein that induces a slow voltage-gated potassium current. *Science* **242**, 1042–1045.

TATHAM, P. E. R. & LINDAU, M. (1990). ATP-induced pore formation in the plasma membrane of rat peritoneal mast cells. *Journal of General Physiology* **95**, 459–475.

THEODOSIS, D. T., LEGENDRE, P. & VINCENT, J. D. (1983). Immunocytochemically identified vasopressin neurons in culture show slow, calcium-dependent electrical responses. *Science* **221**, 1052–1054.

THORN, P. J., WANG, X. & LEMOS, J. R. (1991). A fast, transient K^+ current in neurohypophysial nerve terminals of the rat. *Journal of Physiology* **432**, 313–326.

TZOUNOPOULOS, T., GUY, H. R., DURELL, S., ADELMAN, J. P. & MAYLIE, J. (1995). min K channels form by assembly of at least 14 subunits. *Proceedings of the National Academy of Sciences of the USA* **92**, 9593–9597.

VANDESANDE, F. & DIERICKX, K. (1975). Identification of the vasopressin producing and of the oxytocin producing neurons in the hypothalamic magnocellular neurosecretory system of rat. *Cell and Tissue Research* **164**, 153–162.

VARNUM, M. D., BUSCH, A. E., BOND, C. T., MAYLIE, J. & ADELMAN, J. P. (1993). The min K channel underlies the cardiac potassium current I_{Ks} and mediates species-specific responses to protein kinase C. *Proceedings of the National Academy of Sciences of the USA* **90**, 11528–11532.

WANG, G., THORN, P. & LEMOS, J. R. (1992). A novel large-conductance Ca^{2+}-activated potassium channel and current in nerve terminals of the rat neurohypophysis. *Journal of Physiology* **457**, 47–74.

WANG, G., TREISTMAN, S. N. & LEMOS, J. R. (1993). A novel method for identification of peptide contents from individual neurohypophysial terminals after patch-clamp recordings. *Annals of the New York Academy of Sciences* **689**, 550–553.

WANG, K. & GOLDSTEIN, S. A. N. (1995). Subunit composition of minK potassium channels. *Neuron* **14**, 1303–1309.

Acknowledgements

We wish to thank Wolf Almers for valuable comments on the manuscript. This work was supported by a Max-Planck fellowship and by the Deutsche Forschungsgemeinschaft (DFG Li443/9-1).

Author's present address

G. Kilic: Department of Physiology, University of Colorado Medical School, 4200 East 9-th Avenue, Denver, CO 80262, USA.

Author's email address

M. Lindau: lindau@mzf.mpimf-heidelberg.mpg.de

Received 28 June 1996; accepted 19 September 1996.